LETTERS

LKB1 modulates lung cancer differentiation and metastasis

Hongbin Ji[1,4]*, Matthew R. Ramsey[10,12]*, D. Neil Hayes[11], Cheng Fan[10], Kate McNamara[1,4], Piotr Kozlowski[5], Chad Torrice[11], Michael C. Wu[3], Takeshi Shimamura[1], Samanthi A. Perera[1,4], Mei-Chih Liang[1,4], Dongpo Cai[1], George N. Naumov[8], Lei Bao[13], Cristina M. Contreras[14], Danan Li[1,4], Liang Chen[1,4], Janakiraman Krishnamurthy[10,11], Jussi Koivunen[1], Lucian R. Chirieac[6], Robert F. Padera[6], Roderick T. Bronson[9], Neal I. Lindeman[6], David C. Christiani[2], Xihong Lin[3], Geoffrey I. Shapiro[1,7], Pasi A. Jänne[1,7], Bruce E. Johnson[1,7], Matthew Meyerson[1,15], David J. Kwiatkowski[5], Diego H. Castrillon[14], Nabeel Bardeesy[16], Norman E. Sharpless[10,11,12] & Kwok-Kin Wong[1,7]

Germline mutation in serine/threonine kinase 11 (*STK11*, also called *LKB1*) results in Peutz–Jeghers syndrome, characterized by intestinal hamartomas and increased incidence of epithelial cancers[1]. Although uncommon in most sporadic cancers[2], inactivating somatic mutations of *LKB1* have been reported in primary human lung adenocarcinomas and derivative cell lines[3–5]. Here we used a somatically activatable mutant Kras-driven model of mouse lung cancer to compare the role of *Lkb1* to other tumour suppressors in lung cancer. Although Kras mutation cooperated with loss of *p53* or *Ink4a/Arf* (also known as *Cdkn2a*) in this system, the strongest cooperation was seen with homozygous inactivation of *Lkb1*. *Lkb1*-deficient tumours demonstrated shorter latency, an expanded histological spectrum (adeno-, squamous and large-cell carcinoma) and more frequent metastasis compared to tumours lacking *p53* or *Ink4a/Arf*. Pulmonary tumorigenesis was also accelerated by hemizygous inactivation of *Lkb1*. Consistent with these findings, inactivation of *LKB1* was found in 34% and 19% of 144 analysed human lung adenocarcinomas and squamous cell carcinomas, respectively. Expression profiling in human lung cancer cell lines and mouse lung tumours identified a variety of metastasis-promoting genes, such as NEDD9, VEGFC and CD24, as targets of LKB1 repression in lung cancer. These studies establish LKB1 as a critical barrier to pulmonary tumorigenesis, controlling initiation, differentiation and metastasis.

Non-small-cell lung cancer (NSCLC) is subdivided into three subtypes: squamous cell carcinoma (SCC, ~28%), large-cell carcinoma (LCC, ~24%) and adenocarcinoma (~48%)[6]. Although these differ histologically[7], each is highly lethal and, until recently, little clinical distinction was made among sub-types. Concomitant *KRAS* (v-Ki-ras2 Kirsten rat sarcoma viral oncogene homologue) activation and *LKB1* inactivation occur in lung adenocarcinoma[3], yet $Lkb1^{-/-}$ mouse embryo fibroblasts are resistant to transformation by oncogenic *Ras* (ref.8), and mutations in *RAS* are rare in colonic polyps of Peutz–Jeghers syndrome (PJS) patients[9]. Given this tissue-specific relationship between *KRAS* activation and *LKB1* deficiency, we investigated the tumour suppressor function of Lkb1 in the context of *Kras* activation in an *in vivo* mouse lung cancer model.

To discern relationships among pulmonary tumour suppressor mechanisms, we intercrossed a conditionally activatable *Lox-Stop-Lox* $Kras^{G12D}$ (hereafter called *Kras*) allele[10] and four conditional (L/L) or germline null (−/−) alleles: $Lkb1^{L/L}$, $p53^{L/L}$, $Ink4a/Arf^{-/-}$ and $p16^{Ink4a-/-}$ (refs 8, 11–13). Mice were inoculated with adenoviral CRE (*adeno-Cre*) by inhalation, transducing a small percentage of pulmonary cells[10] (Supplementary Fig. 1). As previously described[10,14–16], mice with Kras activation developed tumours with high multiplicity, long latency and low aggressiveness (Table 1 and Supplementary Fig. 2). In contrast, concomitant $p16^{Ink4a}$ and *p53* inactivation in animals lacking the *Kras* allele produced infrequent, highly lethal tumours. Kras activation cooperated potently with *p53* loss in lung tumorigenesis (Table 1, ref. 16), but only modestly with specific $p16^{Ink4a}$ loss or combined *Ink4a/Arf* loss (Table 1); this indicates that the Kras mutation initiates tumorigenesis, whereas $p16^{Ink4a}$ and p53 constrain tumour progression.

Surprisingly, the strongest genetic interaction was *Kras* mutation combined with homozygous *Lkb1* inactivation (Table 1 and Supplementary Fig. 2). Although caution is warranted in comparing cohorts of mixed genetic backgrounds, median survival for *Kras* $Lkb1^{L/L}$ or *Kras* $Lkb1^{L/-}$ mice was 9 weeks after *adeno-Cre*-inoculation, compared with 14 weeks in *Kras* $p53^{L/L}$ mice. Cooperation was also noted between Kras activation and heterozygous *Lkb1* inactivation, although loss of the wild-type allele was not seen in tumours of heterozygous mice (see below). Inactivation of *Lkb1* in the absence of Kras activation was insufficient for pulmonary neoplasia, establishing that Lkb1 potently suppresses Kras-directed lung tumorigenesis *in vivo*.

Kras $Lkb1^{L/-}$ or *Kras* $Lkb1^{L/L}$ mice demonstrated significantly increased tumour burden at early time points (Fig. 1a and Supplementary Fig. 2) and larger (>3 mm) lesions at later time points than *Kras* mice (Fig. 1b). As previously reported[10,15,16], we did not detect metastasis or local invasion in *Kras* mice. Regional lymph-node metastases were observed in 7 of 22 *Kras* $Lkb1^{+/-}$ or *Kras* $Lkb1^{L/+}$ mice, and in 27 of 44 *Kras* $Lkb1^{L/L}$ or *Kras* $Lkb1^{L/-}$ mice, and axial skeleton metastases were found in 1 *Kras* $Lkb1^{+/-}$ and in 4 *Kras* $Lkb1^{L/L}$ or *Kras* $Lkb1^{L/-}$ mice (Table 1 and Supplementary Fig. 2).

[1]Department of Medical Oncology, Dana-Farber Cancer Institute, [2]Department of Environmental Health, [3]Department of Biostatistics, Harvard School of Public Health, [4]Ludwig Center at Dana-Farber/Harvard Cancer Center, [5]Division of Translational Medicine, [6]Department of Pathology, [7]Department of Medicine, Brigham and Women's Hospital, [8]Department of Surgery, Children's Hospital, [9]Department of Pathology, Harvard Medical School, Boston, Massachusetts 02115, USA. [10]Department of Genetics, [11]Department of Medicine, [12]Curriculum in Genetics and Molecular Biology, The Lineberger Comprehensive Cancer Center, The University of North Carolina School of Medicine, Chapel Hill, North Carolina 27599, USA. [13]Department of Molecular Sciences, University of Tennessee Health Science Center, Memphis, Tennessee 38163, USA. [14]Department of Pathology and Simmons Comprehensive Cancer Center, University of Texas Southwestern Medical Center, Dallas, Texas 75390-9072, USA. [15]Broad Institute of Harvard University and Massachusetts Institute of Technology, Cambridge, Massachusetts 02142, USA. [16]Massachusetts General Hospital Cancer Center, Massachusetts General Hospital, Boston, Massachusetts 02114, USA.
*These authors contributed equally to this work.

Table 1 | Comparison of lung cancer cohorts

Genotype	Number treated	Median survival (weeks)*	Tumour multiplicity†	Squamous or mixed histology	Metastasis	Comments
Kras	26	24	Medium	0 of 16	0 of 19	See also refs 10, 14, 15
Lkb1$^{L/-}$ or *Lkb1*$^{L/L}$	15	>40	NA	NA	NA	No tumours observed
p53$^{L/L}$	16	>40	NA	0 of 1	NA	See also ref. 18
p16$^{Ink4a-/-}$ *p53*$^{L/L}$	15	29	Low	0 of 5	NA	High frequency of fatal pulmonary haemorrhage
Kras p16$^{Ink4a-/-}$	19	24	Medium	0 of 12	3 of 15 (20%)	
Kras p53$^{L/L}$	17	14	High	0 of 9	4 of 9 (44%)	Compare with ref. 16; see also refs 14, 17
Kras Ink4a/Arf$^{-/-}$	26	22	High	0 of 11	0 of 11	Compare with ref. 16
Kras Lkb1$^{L/+}$ or *Kras Lkb1*$^{+/-}$	27	19	High	0 of 18	7 of 22 (32%)	
Kras Lkb1$^{L/L}$ or *Kras Lkb1*$^{L/-}$	56	9	High	15 of 27 (56%)	27 of 44 (61%)	2 of 27 mice also demonstrated large-cell histology

NA, not applicable.
* Median latency shown is after *adeno-Cre* treatment at 5–6 weeks of age, estimated by Kaplan–Meier analysis.
† Tumour multiplicity: low, <3 per lung section; medium, 3–10 per lung section; high, >10 per lung section.

These results indicate that reduced *Lkb1* gene dosage facilitates progression and metastasis in Kras-induced lung cancers.

Consistent with previous reports[10,14–18], all tumours from *Kras* mice with or without *p16*^{Ink4a}, *Ink4a/Arf* or *p53* inactivation were adenocarcinomas. In contrast, 15 of 27 *adeno-Cre*-treated *Kras Lkb1*$^{L/L}$ or *Kras Lkb1*$^{L/-}$ mice harboured SCCs or adenosquamous carcinomas whereas 2 of 27 lungs showed LCCs (Table 1, Fig. 1c). Squamous tumours from *Kras Lkb1*$^{L/L}$ or *Kras Lkb1*$^{L/-}$ mice did not express pro-surfactant protein C (SP-C), a marker of type II pneumocytes and adenocarcinomas, but expressed pan-keratin and p63, markers of SCC. SP-C expression was high and expression of pan-keratin and p63 was low or absent in adenocarcinomas (Fig. 1d, e). Therefore, Lkb1 inactivation facilitated tumours of all three human histological subtypes.

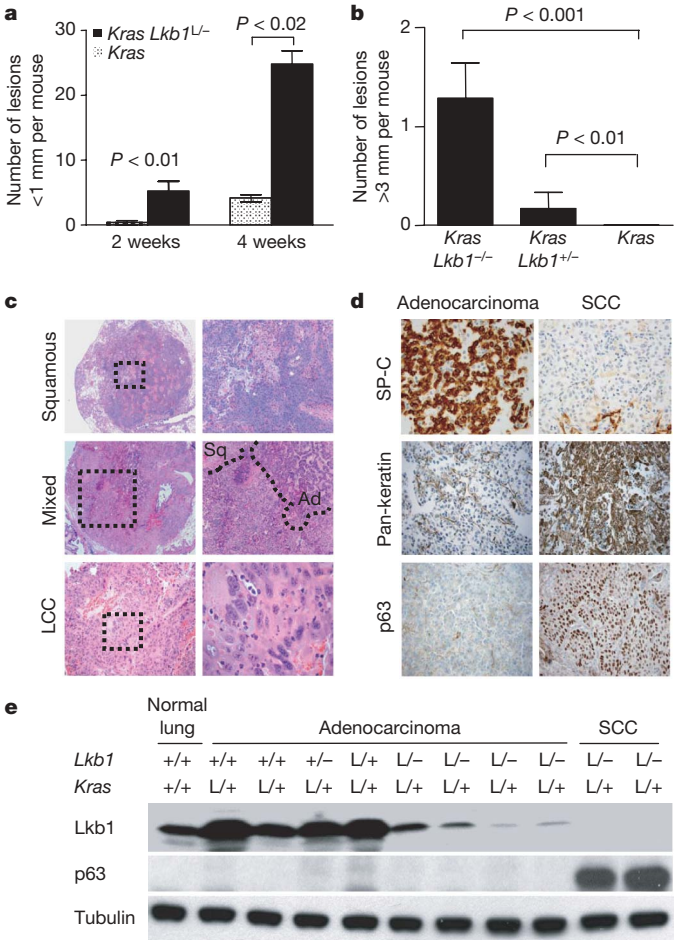

Figure 1 | Lung tumours in *Kras* and *Kras Lkb1*$^{L/L}$ mice. **a**, Quantification of lesions (<1 mm) found in *Kras* or *Kras Lkb1*$^{L/-}$ mice two and four weeks after *adeno-Cre* treatment. $n = 4$–6 for each group. Data are shown as mean ± s.e.m. **b**, Quantification of tumours (>3 mm) in *Kras Lkb1*$^{L/-}$ ($n = 12$), *Kras Lkb1*$^{+/-}$ ($n = 8$) and *Kras* ($n = 10$) mice 8 weeks after *adeno-Cre* treatment. Data are shown as mean ± s.e.m. **c**, Representative lung tumours from *Kras Lkb1*$^{L/-}$ mice showing squamous (top), mixed (middle; Ad, adenocarcinoma; Sq, SCC) or large-cell (bottom) histology. The dotted box in the left image shows the area shown on the right. **d**, Immunohistochemical staining for SP-C, pan-keratin and p63 in adenocarcinomas (left) or in squamous tumours (right) from *Kras Lkb1*$^{L/-}$ or *Kras Lkb1*$^{L/L}$ mice. **e**, Western blot of Lkb1 and p63 expression in tumours from mice of indicated genotype and histology. Histology is indicated as normal lung, adenocarcinoma or SCC. Tubulin serves as a loading control.

To determine whether this mouse model recapitulated genetic events in human NSCLC, we assessed 144 human NSCLCs (Supplementary Table 1) for *KRAS* and *LKB1* mutations by direct exon sequencing, and investigated *LKB1* copy number status by multiplex ligation-dependent probe amplification[19] (Supplementary Fig. 3). In accordance with other studies[3–5], 34% (27 of 80) adenocarcinomas harboured *LKB1* genomic alterations, predominantly (19 of 80) single-copy mutation or deletion (Table 2). *LKB1* alteration was seen in SCCs (8 of 42, 19%) with the predominant lesion (6 of 42) also being single-copy mutation or deletion. Additionally, *LKB1* alteration was found in 1 of 7 LCCs and 1 of 4 adenosquamous carcinomas. *KRAS* mutation has been reported in all subtypes of lung cancer[2] (Supplementary Table 2), and a subset of *LKB1* mutant adenocarcinoma and SCC also contained *KRAS* point mutations (Supplementary Tables 3–5). The frequent occurrence of single-copy mutation or deletion of *LKB1* in human tumours is consistent with the increased rate of tumour formation observed in *Kras Lkb1*$^{+/-}$ or *Kras Lkb1*$^{L/+}$ mice compared to *Kras* mice (Supplementary Fig. 2 and Table 2). Thus, inactivating mutations of *LKB1* are found in all histologic subtypes of human NSCLC.

The tumour-suppressor activity of LKB1 has been reported to function through activation of *p53* and/or the *Ink4a/Arf* locus[3,8,20]. Although we confirmed an effect of *Lkb1* loss on p16^{Ink4a} and Arf expression in mouse embryo fibroblasts (Supplementary Fig. 4), several lines of evidence indicate Lkb1 also harbours *p53*- and *Ink4a/Arf*-independent tumour suppressor roles. Cooperation between *Lkb1* loss and Kras activation in mouse lung cancers was stronger than seen with loss of *p53* or *Ink4a/Arf* (Table 1). Moreover, *Lkb1*-deficient mouse tumours demonstrated enhanced metastasis and squamous differentiation—features not seen in the *p53*- or *Ink4a/Arf*-deficient backgrounds. A substantial fraction of human NSCLC harboured concomitant *p53* and *LKB1* mutation (Supplementary Tables 3–6), suggesting non-redundant roles in NSCLC. Lastly, LKB1 reconstitution in human NSCLC cell lines lacking functional p16^{INK4a}, ARF and p53 demonstrated anti-tumour effects (see below). These data indicate that LKB1 shows anti-tumour activity independent of p16^{INK4a}, ARF and p53.

We performed unsupervised gene expression analysis of mouse primary lung tumours to elucidate previously unknown tumour-suppressor effects of Lkb1. Twenty-five tumours from 20 *Kras* mice of the indicated histologies and *Lkb1* genotypes were analysed using Affymetrix arrays (Supplementary Fig. 5, Supplementary Table 7 and

Table 2 | *LKB1* mutation incidence in human primary NSCLC samples

	Adenocarcinoma	SCC	Other*	Total
Only point mutation or deletion	8 of 80 (10)	4 of 42 (10)	1 of 22 (5)	13 of 144 (9)
Only single-copy loss by MLPA	11 of 80 (14)	2 of 42 (5)	1 of 22 (5)	14 of 144 (10)
Homozygous mutation or deletion	8† of 80 (10)	2 of 42 (5)	0 of 22 (0)	10 of 144 (7)
Total	27 of 80 (34)	8 of 42 (19)	2 of 22 (9)	37 of 144 (26)

Shown is the fraction of NSCLC samples studies found to harbour an *LKB1* mutation of the indicated class. Numbers in parentheses represent per cent.
* LCCs, adenosquamous carcinomas and NSCLCs of unknown subtype.
† Includes four samples with single-copy-loss by MLPA and point mutation by sequencing.

Supplementary Data 1). The most distinct group of tumours (tumours R–T) was comprised of squamous or adenosquamous (mixed) tumours from *Kras Lkb1*$^{L/-}$ mice, which showed marked increases in the expression of genes (for example, p63, Krt5/6, desmoplakin; cluster A) overexpressed in human squamous lung cancer versus adenocarcinoma[7,21]. These tumours also demonstrated sharply reduced expression of the *Lkb1* transcript and protein (Fig. 1e and data not shown). Therefore, in a subset of Kras-induced mouse tumours, loss of *Lkb1* expression was associated with the overexpression of transcripts characteristic of human SCCs.

Adenocarcinomas clustered into two groups on the basis of *Lkb1* status. Tumours A–L from *Kras Lkb1*$^{+/+}$ mice showed high expression of *Lkb1* and transcripts associated with carbohydrate and lipid metabolism (Supplementary Fig. 5), consistent with the role of Lkb1 in regulating the nutrient-sensing AMPK pathway[22]. These tumours showed increased phosphorylation of AMPK and ACC compared to adenocarcinoma tumours from *Kras Lkb1*$^{L/+}$ or *Kras Lkb1*$^{L/-}$ mice, which were characterized by reduced expression of *Lkb1* and reduced phospho-AMPK and phospho-ACC (Supplementary Fig. 6). These data indicate that Lkb1 influences AMPK activation and expression of a large number of genes within the tumour subtype of Ras-driven adenocarcinoma.

Metastases from animals in all cohorts appeared adenocarcinoma-like, and squamous-like metastases were not seen. Accordingly, the *Lkb1*-deficient adenocarcinomas demonstrated increased expression of genes thought to promote angiogenesis and/or metastasis such as *Nedd9*, *Vegfc*, *Loxl1*, *Pdgf* receptor and *Mmp2*, which were not increased in *Lkb1*-deficient squamous tumours (Supplementary Fig. 5). This indicates that Lkb1 loss facilitates metastasis and permits squamous differentiation, but these effects appear genetically separable.

To understand the mechanism whereby LKB1 suppresses metastasis, we stably expressed equivalent amounts of either wild-type LKB1 or kinase-dead LKB1(K78I) (LKB1-KD) in LKB1-deficient NSCLC lines A549 or H2126 (Fig. 2a). Similar to a previous report on a breast cancer cell line[23], LKB1 potently suppressed anchorage-independent growth in soft agar (Fig. 2b) and pulmonary metastases after tail-vein injection (Fig. 2c). Notably, LKB1 reconstitution in the A549 line did not affect the expression of p53, p53 targets or the p53 response to ultraviolet radiation (Supplementary Fig. 7). Because this line harbours homozygous *INK4a/ARF* inactivation, this result demonstrates that the anti-metastatic effect of LKB1 is *INK4a/ARF*- and *p53*-independent.

To refine the transcriptional analysis of *Lkb1*-deficient mouse tumours, A549 and H2126 cells with and without LKB1 reconstitution were analysed by unsupervised expression profiling (Supplementary Fig. 8 and Supplementary Data 2). Only a small number of genes demonstrated reduced expression in both A549 and H2126 lines with LKB1 reconstitution (Supplementary Fig. 8). Combined analysis of these human cell lines and *Lkb1*$^{-/-}$ mouse tumours identified *NEDD9* as an LKB1-regulated transcript (Supplementary Figs 5 and 8), and a previous study has shown a role for NEDD9 in metastasis[24]. Protein expression of NEDD9 in A549 and H2126 cell lines was repressed by wild-type LKB1, but not LKB1-KD (Fig. 2a), and increased *Nedd9* expression was noted in adenocarcinomas from *Kras Lkb1*$^{L/L}$ or *Kras Lkb1*$^{L/-}$ mice compared to adenocarcinomas from Kras mice or squamous tumours from *Kras Lkb1*$^{L/L}$ or *Kras Lkb1*$^{L/-}$ (Fig. 2d). In addition, 70–80% reduction in NEDD9 levels by short hairpin RNA (shRNA) in A549 cells reduced migration and invasion by more than 60% in Boyden chamber assays (Fig. 2e), suggesting that NEDD9 is an important mediator of metastasis in mouse and human NSCLCs lacking LKB1.

Although LKB1 negatively regulates the mTOR pathway[25] (Fig. 2a and Supplementary Fig. 6), treatment of parental A549 cells with rapamycin, an mTOR inhibitor, had no effect on NEDD9 protein levels, despite a clear decrease in both S6 kinase and S6 ribosomal protein phosphorylation (Supplementary Fig. 9). This indicates that either NEDD9 is a very stable protein ($T_{1/2} > 72$ h) or it is repressed by LKB1 in an mTOR-independent manner.

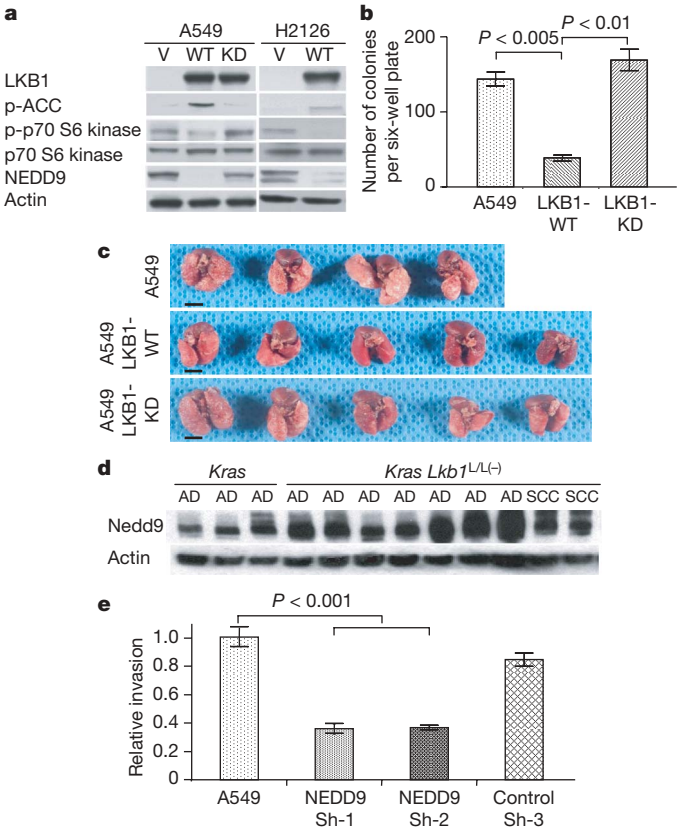

Figure 2 | LKB1 suppresses metastasis. a, A549 and H2126 cells were stably transduced with pBABE-puro (V), pBABE-LKB1 (WT) or kinase dead pBABE-LKB1(K78I) (KD) and were assessed for expression of indicated genes by western blotting. Actin serves as a loading control. **b**, A549 cell lines were assessed for the ability to form colonies in soft agar. Data are shown as average number of colonies per six-well plate after 14 days ($n = 4$) and error bars represent s.e.m. **c**, A549 cell lines were injected into SCID mice by way of tail vein, and lung seeding was analysed eight weeks post-injection. Representative photographs of lungs are shown. **d**, Lung tumours from *Kras* or *Kras Lkb1*$^{L/L}$ or *Kras Lkb1*$^{L/-}$ mice were assessed for expression of Nedd9. Actin serves as a loading control. Tumour histology is indicated as adenocarcinoma (AD), adeno–squamous mixed (AS) or SCC. **e**, A549 parental cells and A549 stably transduced cells with two different shRNAs against NEDD9 (Sh-1 and Sh-2) or control shRNA (Sh-3) were subjected to analyses with CytoSelect Cell Invasion assay. Invasion is plotted relative to A549 parental cell lines. Data are shown as mean ± s.e.m. ($n = 6$).

The LKB1 reconstitution experiments suggest that LKB1 modulates differentiation in NSCLC cell lines. In H2126 cells, LKB1 reproducibly altered the expression of hundreds of genes in independent experiments (Supplementary Fig. 8 and Supplementary Data 2). In particular, LKB1 restoration repressed characteristic luminal squamous epithelial markers such as keratins 8 and 18 and desmoplakin, and increased expression of adenomatous transcripts such as surfactants A, A2 and B (Supplementary Fig. 10). Intriguingly, LKB1 also increased expression of 'basal' markers such as Trp63 (also called p63 and p73L) and keratins 5, 6 and 17, and reduced expression of CD24—a luminal marker differentially regulated in putative breast and pancreatic carcinoma stem cells[26–28]. CD24 was expressed in *Lkb1*-deficient squamous mouse tumours and in some adenocarcinomas (tumours O, P and R–T; Supplementary Fig. 5), and was repressed by LKB1 in A549 and H2126 cell lines (Supplementary Fig. 11). Given these results, it is tempting to speculate that LKB1 inactivation influences lineage choice in a common lung cancer progenitor cell.

We have described a mouse model of lung SCCs and have demonstrated repressive functions of LKB1 on metastasis through regulation of NEDD9. We find that LKB1 inactivation is frequent in all human NSCLC subtypes, suggesting similar tumour-suppressor roles in humans. Furthermore, our mouse data predict that LKB1 loss will serve as a prognostic marker of adverse disease. In accordance with this view, in ref. 29 it was recently noted that *LKB1* mutation correlates with advanced disease in NSCLCs, including SCCs. These data establish that LKB1 suppresses lung tumorigenesis through at least three independent mechanisms influencing tumour initiation, differentiation and metastasis.

METHODS SUMMARY

Kras mice were provided by T. Jacks, and were treated with 5×10^6 p.f.u. *adeno-Cre* (University of Iowa adenoviral core) intranasally as previously described[10]. For human tumour analysis, surgically resected human NSCLCs were flash-frozen, and genomic DNA was prepared from frozen tumour samples and sent for direct exon sequencing by Polymorphic DNA Technologies Inc. to detect *LKB1*, *KRAS*, *p53* and $p16^{INK4a}$ mutations. Multiplex ligation-dependent probe amplification (MLPA) was performed as described previously[19]. Histology immunohistochemical and immunoblotting analyses were performed according to standard protocols, as previously described[30]. Cytoselect cell invasion assays were performed as instructed by the manufacturer (Cell Biolabs). A549 cells ($INK4a/ARF^{-/-}$, $LKB1^{-/-}$) and H2126 cells ($INK4a/ARF^{-/-}$, $p53^{-/-}$, $LKB1^{-/-}$) were obtained from ATCC, and soft agar colony formation was assessed as described in Supplementary Data. For lung metastasis analysis, A549 cells or A549 stable cell lines with expression of wild-type LKB1 and LKB1-KD were injected into severe combined immunodeficient (SCID) mice by way of tail veins, and were assessed eight weeks post-inoculation for both gross inspection and histology analysis. For microarray analysis of human and mouse tumours, total RNA was extracted, amplified and labelled by standard methods and hybridized to Agilent 44,000 feature custom-designed Agilent arrays (human tumours) or to Mouse430A2 GeneChip Arrays (Affymetrix) representing 22,690 unique transcripts.

Full Methods and any associated references are available in the online version of the paper at www.nature.com/nature.

Received 15 March; accepted 19 June 2007.
Published online 5 August 2007.

1. Hearle, N. *et al.* Frequency and spectrum of cancers in the Peutz–Jeghers syndrome. *Clin. Cancer Res.* **12,** 3209–3215 (2006).
2. Forbes, S. *et al.* Cosmic 2005. *Br. J. Cancer* **94,** 318–322 (2006).
3. Sanchez-Cespedes, M. *et al.* Inactivation of *LKB1/STK11* is a common event in adenocarcinomas of the lung. *Cancer Res.* **62,** 3659–3662 (2002).
4. Carretero, J., Medina, P. P., Pio, R., Montuenga, L. M. & Sanchez-Cespedes, M. Novel and natural knockout lung cancer cell lines for the *LKB1/STK11* tumor suppressor gene. *Oncogene* **23,** 4037–4040 (2004).
5. Avizienyte, E. *et al. LKB1* somatic mutations in sporadic tumors. *Am. J. Pathol.* **154,** 677–681 (1999).
6. Tuveson, D. A. & Jacks, T. Modeling human lung cancer in mice: similarities and shortcomings. *Oncogene* **18,** 5318–5324 (1999).
7. Hayes, D. N. *et al.* Gene expression profiling reveals reproducible human lung adenocarcinoma subtypes in multiple independent patient cohorts. *J. Clin. Oncol.* **24,** 5079–5090 (2006).
8. Bardeesy, N. *et al.* Loss of the Lkb1 tumour suppressor provokes intestinal polyposis but resistance to transformation. *Nature* **419,** 162–167 (2002).
9. Entius, M. M. *et al.* Peutz–Jeghers polyps, dysplasia, and K-*ras* codon 12 mutations. *Gut* **41,** 320–322 (1997).
10. Jackson, E. L. *et al.* Analysis of lung tumor initiation and progression using conditional expression of oncogenic *K-ras*. *Genes Dev.* **15,** 3243–3248 (2001).
11. Jonkers, J. *et al.* Synergistic tumor suppressor activity of BRCA2 and p53 in a conditional mouse model for breast cancer. *Nature Genet.* **29,** 418–425 (2001).
12. Serrano, M. *et al.* Role of the *INK4a* locus in tumor suppression and cell mortality. *Cell* **85,** 27–37 (1996).
13. Sharpless, N. E. *et al.* Loss of $p16^{Ink4a}$ with retention of $p19^{Arf}$ predisposes mice to tumorigenesis. *Nature* **413,** 86–91 (2001).
14. Johnson, L. *et al.* Somatic activation of the *K-ras* oncogene causes early onset lung cancer in mice. *Nature* **410,** 1111–1116 (2001).
15. Meuwissen, R., Linn, S. C., van der Valk, M., Mooi, W. J. & Berns, A. Mouse model for lung tumorigenesis through Cre/lox controlled sporadic activation of the K-Ras oncogene. *Oncogene* **20,** 6551–6558 (2001).
16. Fisher, G. H. *et al.* Induction and apoptotic regression of lung adenocarcinomas by regulation of a *K-Ras* transgene in the presence and absence of tumor suppressor genes. *Genes Dev.* **15,** 3249–3262 (2001).
17. Jackson, E. L. *et al.* The differential effects of mutant p53 alleles on advanced murine lung cancer. *Cancer Res.* **65,** 10280–10288 (2005).
18. Meuwissen, R. *et al.* Induction of small cell lung cancer by somatic inactivation of both *Trp53* and *Rb1* in a conditional mouse model. *Cancer Cell* **4,** 181–189 (2003).
19. Volikos, E. *et al. LKB1* exonic and whole gene deletions are a common cause of Peutz–Jeghers syndrome. *J. Med. Genet.* **43,** e18 (2006).
20. Karuman, P. *et al.* The Peutz–Jegher gene product LKB1 is a mediator of p53-dependent cell death. *Mol. Cell* **7,** 1307–1319 (2001).
21. Raponi, M. *et al.* Gene expression signatures for predicting prognosis of squamous cell and adenocarcinomas of the lung. *Cancer Res.* **66,** 7466–7472 (2006).
22. Hardie, D. G. New roles for the LKB1→AMPK pathway. *Curr. Opin. Cell Biol.* **17,** 167–173 (2005).
23. Zhuang, Z. G., Di, G. H., Shen, Z. Z., Ding, J. & Shao, Z. M. Enhanced expression of LKB1 in breast cancer cells attenuates angiogenesis, invasion, and metastatic potential. *Mol. Cancer Res.* **4,** 843–849 (2006).
24. Kim, M. *et al.* Comparative oncogenomics identifies NEDD9 as a melanoma metastasis gene. *Cell* **125,** 1269–1281 (2006).
25. Shaw, R. J. *et al.* The LKB1 tumor suppressor negatively regulates mTOR signaling. *Cancer Cell* **6,** 91–99 (2004).
26. Al-Hajj, M., Wicha, M. S., Benito-Hernandez, A., Morrison, S. J. & Clarke, M. F. Prospective identification of tumorigenic breast cancer cells. *Proc. Natl Acad. Sci. USA* **100,** 3983–3988 (2003).
27. Li, C. *et al.* Identification of pancreatic cancer stem cells. *Cancer Res.* **67,** 1030–1037 (2007).
28. Shipitsin, M. *et al.* Molecular definition of breast tumor heterogeneity. *Cancer Cell* **11,** 259–273 (2007).
29. Matsumoto, S. *et al.* Prevalence and specificity of LKB1 genetic alterations in lung cancers. *Oncogene* advance online publication, doi: 10.1038/sj.onc.1210418 (26 March 2007).
30. Ji, H. *et al.* K-ras activation generates an inflammatory response in lung tumors. *Oncogene* **25,** 2105–2112 (2006).

Supplementary Information is linked to the online version of the paper at www.nature.com/nature.

Acknowledgements We thank G. Tonon, C. Perou, W. Kim and the Harvard lung SPORE group for advice and discussions; J. Yokota for sharing unpublished data; and W. Winckler, R. Mukundhan, S. Zaghlul, H. Xia, B. L. Jung, M. Zheng and C. Lam for technical support. We acknowledge the technical assistance of the UNC Tissue Procurement Core Facility, an NCI-designated core laboratory. This work was supported by the NIH (NIA and NCI), the Sidney Kimmel Foundation for Cancer Research (D.H.C., K.-K.W. and N.E.S.), the American Federation of Aging (N.E.S.), the Joan Scarangello Foundation to Conquer Lung Cancer (K.-K.W.), the Flight Attendant Medical Research Institute (K.-K.W.), the Waxman Foundation (N.B.), the Harvard Stem Cell Institute (N.B.), and the Linda Verville Foundation (N.B.).

Author Contributions The laboratories of N.B., N.E.S. and K.-K.W. contributed equally to this work.

Author Information The entire set of unprocessed raw microarray data for both the human and the mouse analyses is available at http://genome.unc.edu and through the Gene Expression Omnibus (GSE6135). Reprints and permissions information is available at www.nature.com/reprints. The authors declare no competing financial interests. Correspondence and requests for materials should be addressed to K.-K.W. (kwong1@partners.org) or N.E.S. (nes@med.unc.edu) or N.B. (nelbardeesy@partners.org).

METHODS

Mouse colony and mouse tumour analysis. All mice were housed and treated in accordance with protocols approved by the institutional care and use committees for animal research at the Dana-Farber Cancer Institute and the University of North Carolina. All cohorts in Table 1 were of a similar, mixed genetic background (~75% C57Bl/6, ~25% FVB/n and 129SvEv). More than 500 mice were analysed in a standard manner for experiments reported in Table 1, but *adeno-Cre*-treated littermates of less informative genotypes (for example, compound heterozygotes, etc.) and animals treated with empty adenovirus are not shown in the interest of brevity. In all cases, heterozygote mice showed tumour-prone phenotypes intermediate to the wild-type and homozygous mutant animals. For CRE expression, 5×10^6 p.f.u. *adeno-Cre* (purchased from University of Iowa adenoviral core) was administered intranasally as previously described[10].

Human tumour analysis. All human studies were approved by the University of North Carolina and Massachusetts General Hospital institutional review boards. Surgically resected human NSCLCs of all clinical stages were flash-frozen and stored at –80 °C until the time of analysis. Samples at University of North Carolina were obtained by means of the Tissue Procurement Facility. Genomic DNA was prepared from frozen tumour samples using Qiagen genomic DNA purification columns and sent for direct exon sequencing by Polymorphic DNA Technologies Inc. to detect *LKB1*, *KRAS*, *p53* and *p16*^{INK4a} mutations. MLPA was performed as described previously[19,31] using the SALSA MLPA kit P101 STK11 (MRC-Holland), which includes 1 probe set for each of the 10 exons of *LKB1*, 5 probe sets extending 0.9 Mb 5′ to LKB1, 1 probe set 10 Mb 3′ to *LKB1*, and 12 control probe sets from elsewhere in the genome. Briefly, 3.4 µl genomic DNA (20 ng µl^{-1}) was incubated at 98 °C for 5 min. After cooling to 21 °C, 1 µl probe mix (containing 1 fmol of probes) and 1 µl SALSA hybridization buffer were added, and the solution was denatured at 95 °C for 2 min and hybridized at 60 °C for 16 h. Hybridized probes were ligated at 54 °C for 15 min by addition of 21 µl ligation mixture. Following heat inactivation, 7.5 µl ligation reaction was mixed with 22.5 µl PCR buffer, heated to 60 °C, mixed with 7.5 µl PCR mixture (SALSA polymerase, dNTPs and universal primers, one of which was labelled with fluorescein) and subjected to PCR amplification for 30 cycles.

Amplification products were diluted in water and then 1:9 in HiDi formamide (ABI) containing 1/36 volume of ROX500 size standard (ABI; final dilution 20-fold), and were then separated by size on an ABI 3100 Genetic Analyser (ABI). Electropherograms were analysed by GeneMapper v3.5 (ABI), and peak height data were exported to an Excel table. Excel programs were used to transform the peak height data to normalized values, such that control samples gave a value of 1 after normalization. Briefly, peak heights for each probe were divided by the average signal from five control probes (on chromosomes 4, 12, 15 and 16), and then that value was divided by a similar value calculated from reference samples. We used the average values from four reference blood DNA samples processed concurrently for each analysis.

Histology and immunohistochemistry. Mice were killed and the left lungs were dissected. The right lung and mediastinal structures were inflated with neutral buffered 10% formalin for 10 min and fixed in 10% formalin overnight at room temperature. Fixed tissues were embedded in paraffin, sectioned at 5 µm, and haematoxylin and eosin stained (Department of Pathology in Brigham and Women's Hospital). Immunohistochemical analyses were performed as described[30]. The antibodies used were: SPC (AB3786, Chemicon), pan-keratin (Z0622, Dako), p63 (ab3239, Abcam), p-AMPK (2535, Cell Signaling), phospho-acetyl-CoA carboxylase (Ser79) (3661, Cell Signaling) and VEGFC (2712, Cell Signaling).

Western blotting and mRNA analysis. Western blot assays were performed as previously described[32] with antibodies against p16^{INK4a} (M-156, Santa Cruz), Arf (ab-80, Abcam), actin (C-1, Santa Cruz), Lkb1 (Clone 5c10, Upstate), Nedd9 (gift of L. Chin), S6 kinase (9202, Cell Signaling), phospho-S6 kinase (9204, Cell Signaling), S6 ribosomal protein (2217, Cell Signaling), phospho-S6 ribosomal protein (2215, Cell Signaling), p21^{CIP1} (F-8, Santa Cruz), phospho-p53 (Cell Signaling), p53 (CM5, Novacastra), phospho-ACC (Cell Signaling), tubulin (clone DM 1A, Sigma-Aldrich), p63 (4892, Cell Signaling) and β-actin (A5441, Sigma). Expression of messenger RNA was analysed by quantitative TaqMan real-time PCR as previously described with some modifications[33]. Reactions were carried out using complementary DNA equivalent to 80 ng RNA and were performed in triplicate for each sample. 18S ribosomal RNA was used as a loading control for all reactions. The primer set for 18S (Hs99999901_s1) was purchased from Applied Biosystems; p16^{INK4a} and Arf primers were generated as previously described[33].

***In vitro* analysis.** A549 cells (*INK4a/ARF*$^{-/-}$, *LKB1*$^{-/-}$) and H2126 cells (*INK4a/ARF*$^{-/-}$, *p53*$^{-/-}$, *LKB1*$^{-/-}$) were obtained from ATCC. To assess soft agar colony formation, parental A549 cells and A549 stable cell lines with expression of wild-type LKB1 and LKB1-KD were suspended in a top layer of RPMI1640 containing 10% FBS and 0.4% Select agar (Gibco/Invitrogen) at 5,000 cells per well in triplicate in 6-well plates and plated on a bottom layer of RPMI1640 containing 10% FBS and 1% Select agar. After 2-week culture, cells were stained with 0.5 ml crystal violet for 1 h. The colonies were then counted in triplicate wells from 10 fields photographed with a ×10 objective. Lentiviral-based shRNA constructs against human NEDD9 (sh-1, CCTCCTTCTCATACCACTCAA; sh-2, CCAGCAGAAACCAGTGAGAAA) were provided by M. Kim and L. Chin.

***In vivo* lung seeding assay of NSCLC cell lines.** Parental A549 cells and A549 stable cell lines with expression of wild-type LKB1 and LKB1-KD were injected into SCID mice intravenously by way of tail veins. After eight weeks of inoculation, the mice were sacrificed and the lungs were dissected for both gross inspection and histology analysis.

Statistical analysis. Tumour-free survival and comparisons of tumour numbers and colonies in soft agar were analysed using Graphpad Prism4. Statistical analyses were performed using nonparametric Mann–Whitney test. Comparisons of mRNA levels were made using the unpaired Student's *t*-test. All data are shown as mean ± s.e.m.

Microarray analysis. For mouse tumours, total RNA was extracted, amplified and labelled by standard methods and hybridized to Mouse430A2 GeneChip Arrays (Affymetrix) representing 22,690 unique transcripts. Probe-level intensity data files in the CEL format (http://www.stat.lsa.umich.edu/~kshedden/Courses/Stat545/Notes/AffxFileFormats/cel.html) were pre-processed using the Robust Multichip Average[34–36] as implemented in Bioconductor (http://www.bioconductor.org/). Gene-expression data were filtered using low stringency, pre-defined criteria: probe set intensity (>32 in all samples) and dynamic variation (more than twofold over the entire sample set). After filtering, multiple probe sets that presented the same genes were collapsed by taking the median value for that gene per array yielding 3,275 unique genes, on which two-way hierarchical clustering was performed (Supplementary Fig. 5). Excerpted clusters are shown in Supplementary Fig. 5, and the list and normalized expression of all 3,275 filtered genes is available as Supplementary Data 1. For human cell lines, total RNA was extracted, amplified and labelled by standard methods and hybridized to Agilent 44,000 feature custom-designed Agilent arrays, which are largely based on the 44,000 feature Agilent Human catalogue arrays, and scanned using an Agilent scanner. Gene expression data were filtered using the same criteria as for the mouse tumours. This filtering strategy yielded 9,644 non-unique transcripts which were then analysed by hierarchical clustering (Supplementary Figs 8 and 10), with excerpted clusters shown. The entire list and normalized expression of all 9,644 filtered transcripts is available as Supplementary Data 2. The entire set of unprocessed raw data for both the human and mouse analyses is available at http://genome.unc.edu and through the Gene Expression Omnibus (GSE6135).

31. Kozlowski, P. *et al.* Identification of 54 large deletions/duplications in TSC1 and TSC2 using MLPA, and genotype–phenotype correlations. *Hum. Genet.* **121,** 389–400 (2007).
32. Sharpless, N. E., Ramsey, M. R., Balasubramanian, P., Castrillon, D. H. & DePinho, R. A. The differential impact of p16(INK4a) or p19(ARF) deficiency on cell growth and tumorigenesis. *Oncogene* **23,** 379–385 (2004).
33. Krishnamurthy, J. *et al.* p16INK4a induces an age-dependent decline in islet regenerative potential. *Nature* **443,** 453–457 (2006).
34. Irizarry, R. A. *et al.* Summaries of Affymetrix GeneChip probe level data. *Nucleic Acids Res.* **31,** e15 (2003).
35. Irizarry, R. A. *et al.* Exploration, normalization, and summaries of high density oligonucleotide array probe level data. *Biostatistics* **4,** 249–264 (2003).
36. Bolstad, B. M., Irizarry, R. A., Astrand, M. & Speed, T. P. A comparison of normalization methods for high density oligonucleotide array data based on variance and bias. *Bioinformatics* **19,** 185–193 (2003).

Whole Mount

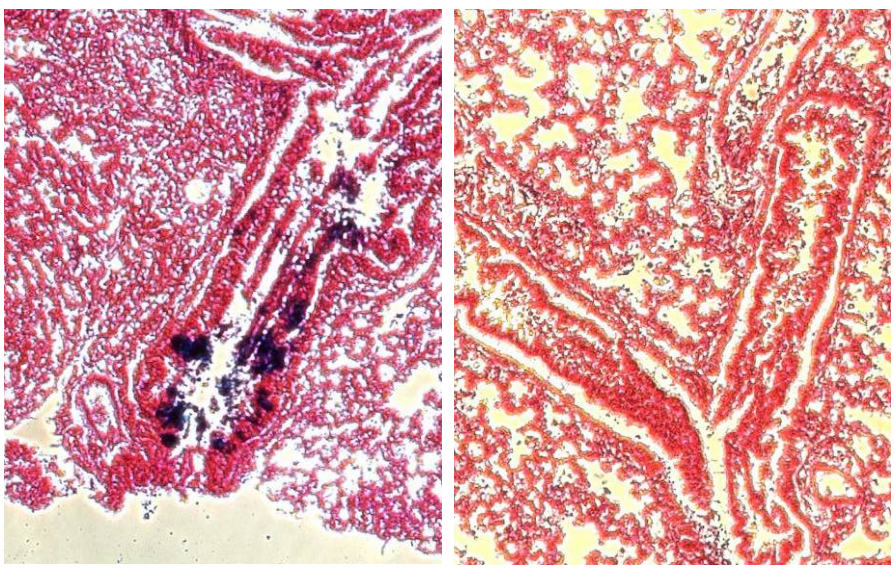

Original Magnification 200X

Adeno-CRE **Adeno-Empty**

Ji, Ramsey et al., Supplementary Figure 1

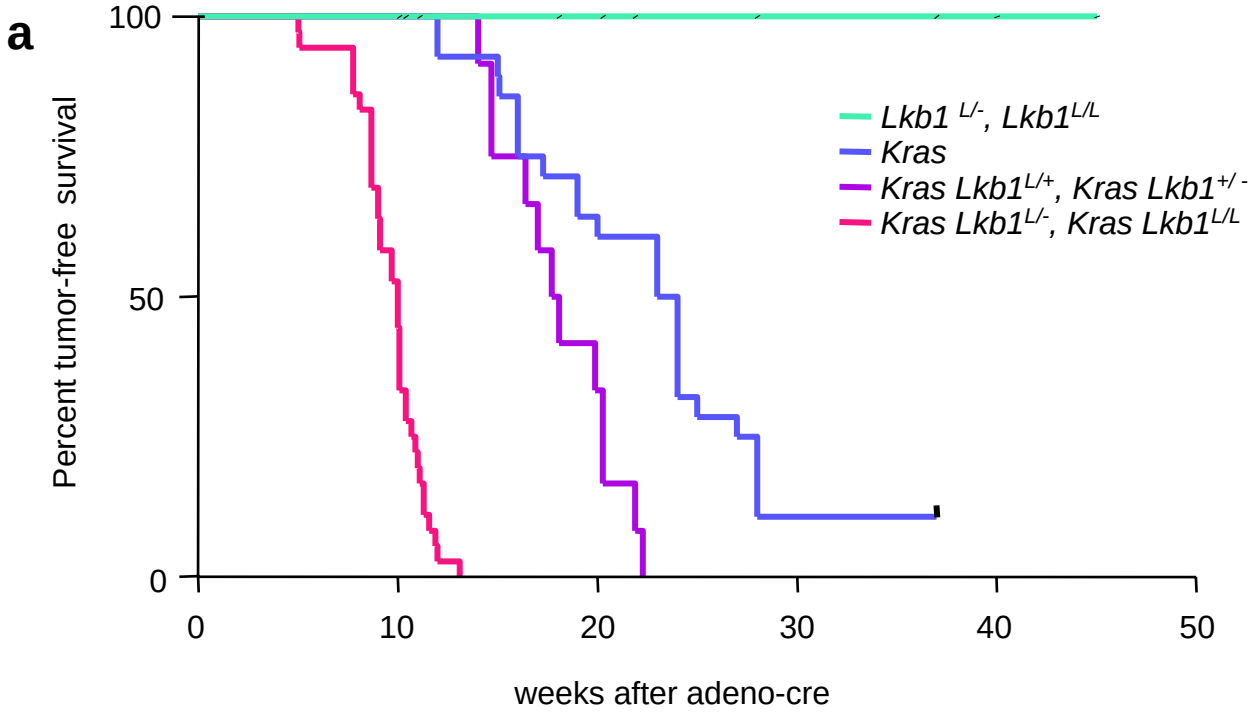

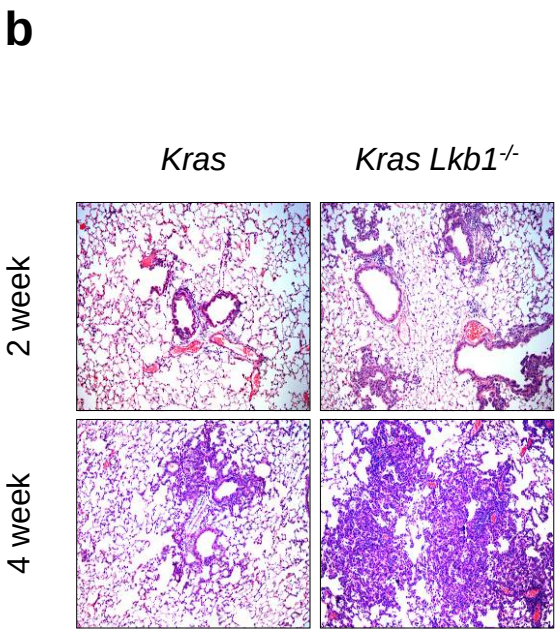

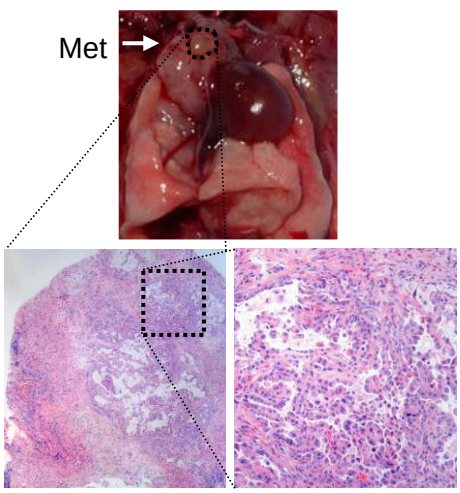

Ji, Ramsey et al., Supplementary Figure 2

a

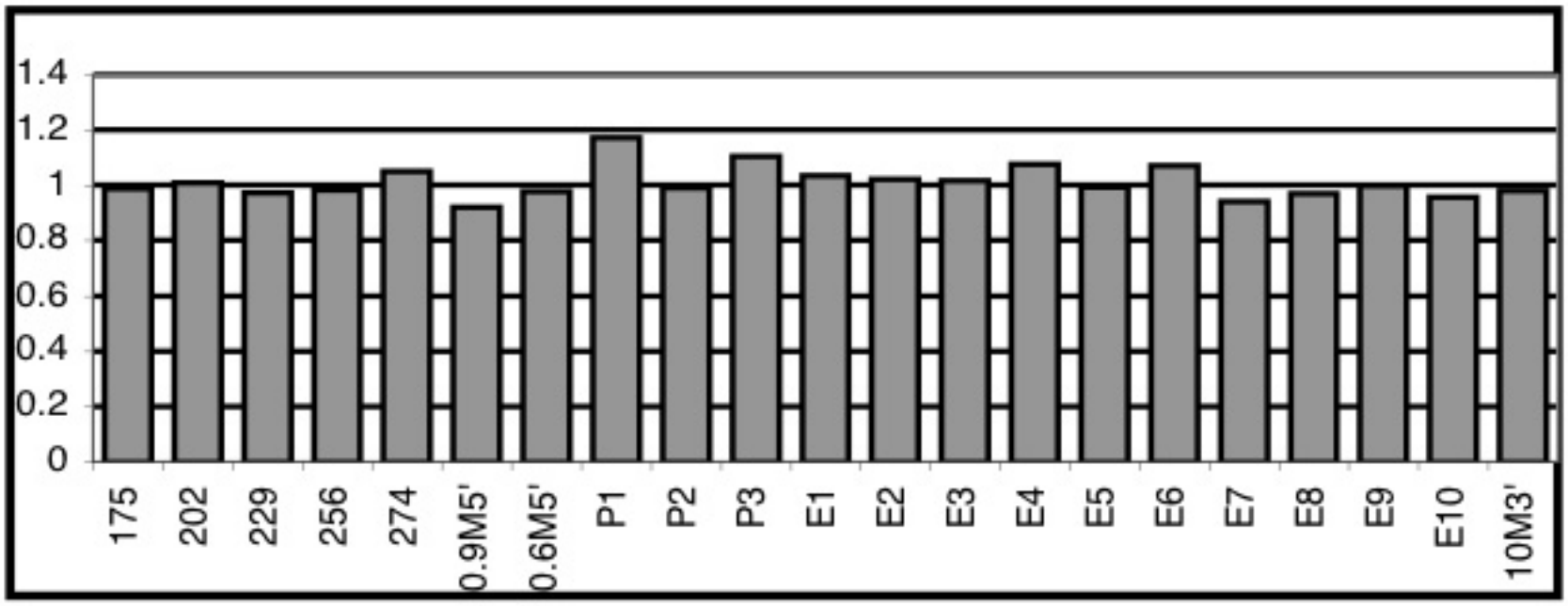

b

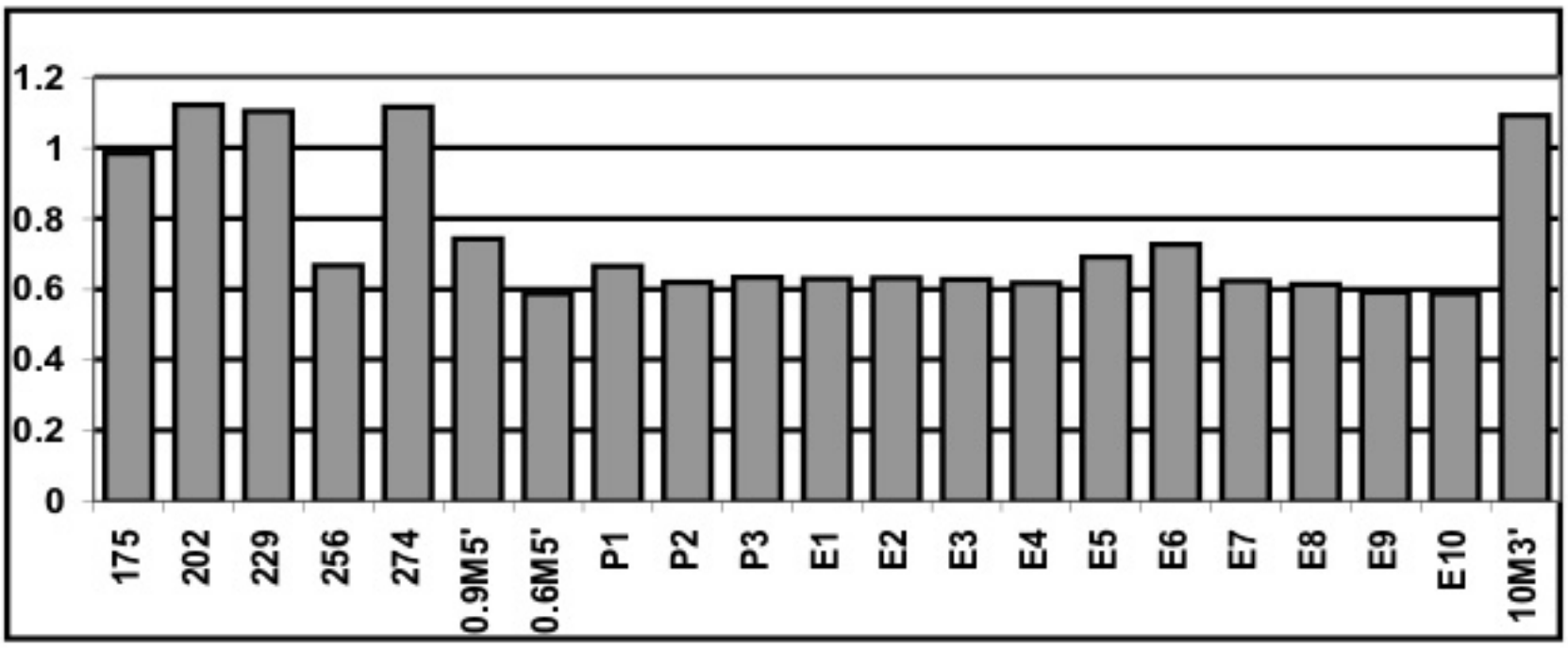

C

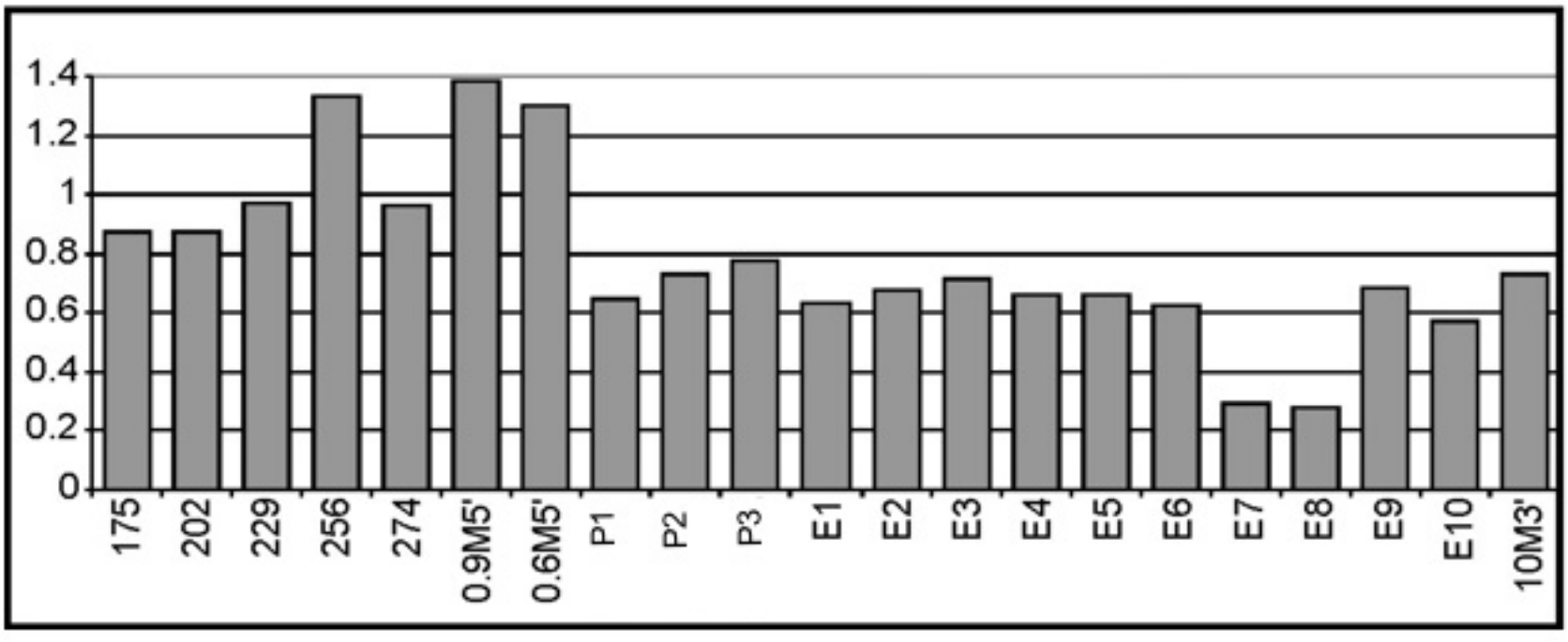

Ji, Ramsey et al., Supplementary Figure 3

a

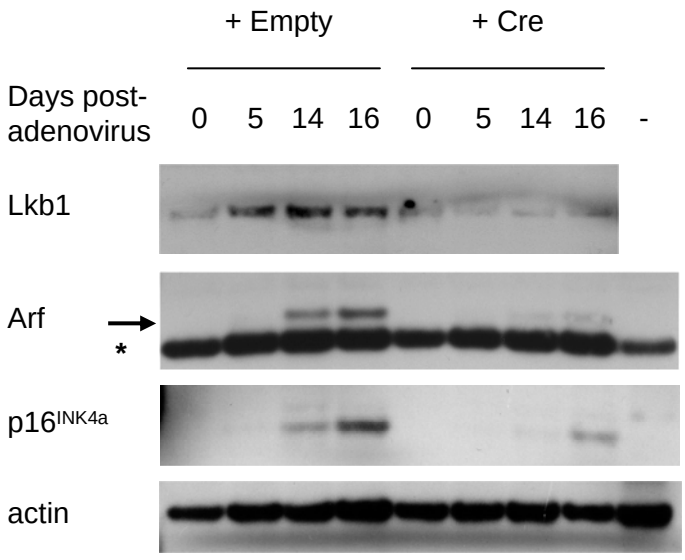
+ Empty
+ Cre
Days post-adenovirus
0 5 14 16 0 5 14 16 -
Lkb1
Arf
*
p16INK4a
actin

b

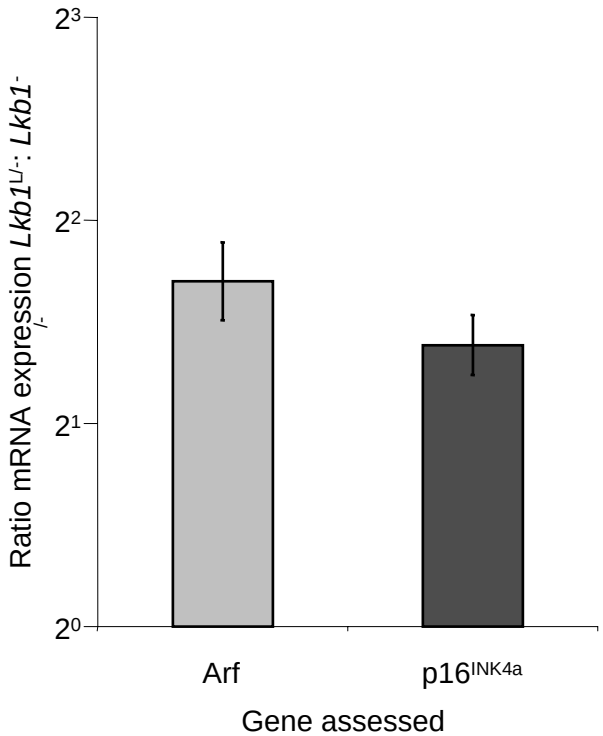
Ratio mRNA expression Lkb1L-/-: Lkb1-/-
2^3
2^2
2^1
2^0
Arf
p16INK4a
Gene assessed

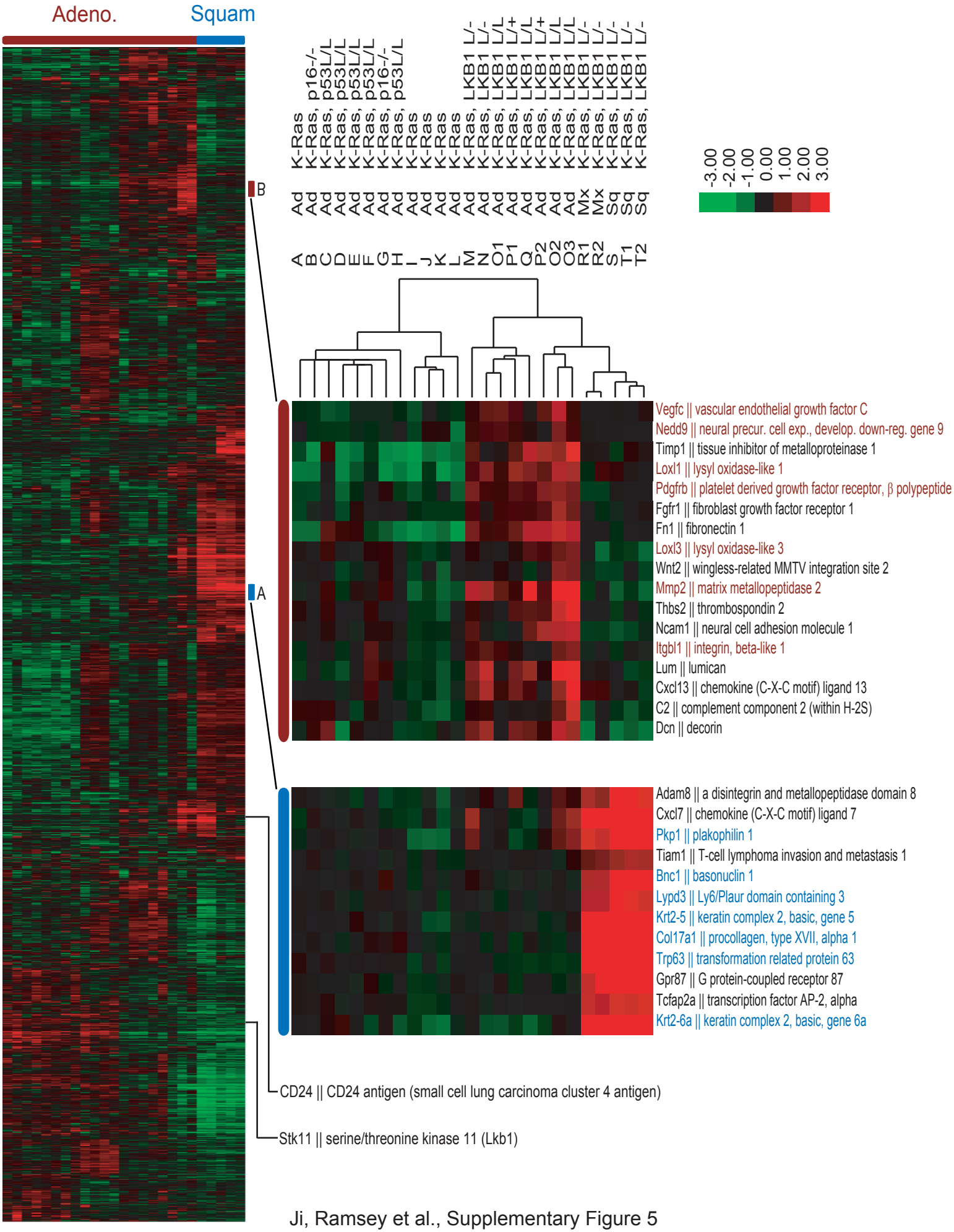

Ji, Ramsey et al., Supplementary Figure 5

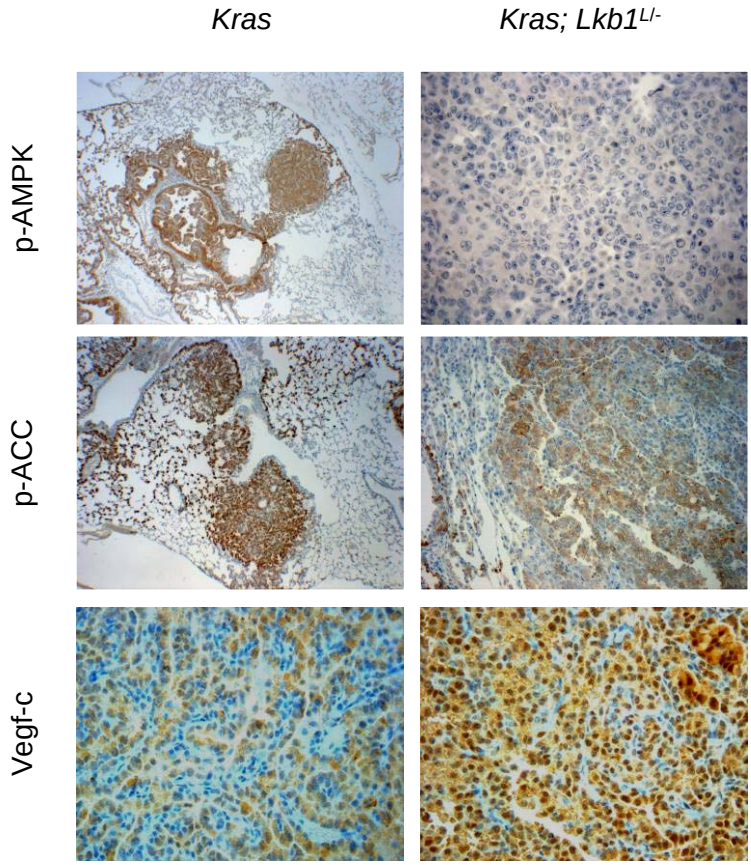

Ji, Ramsey et al., Supplementary Figure 6

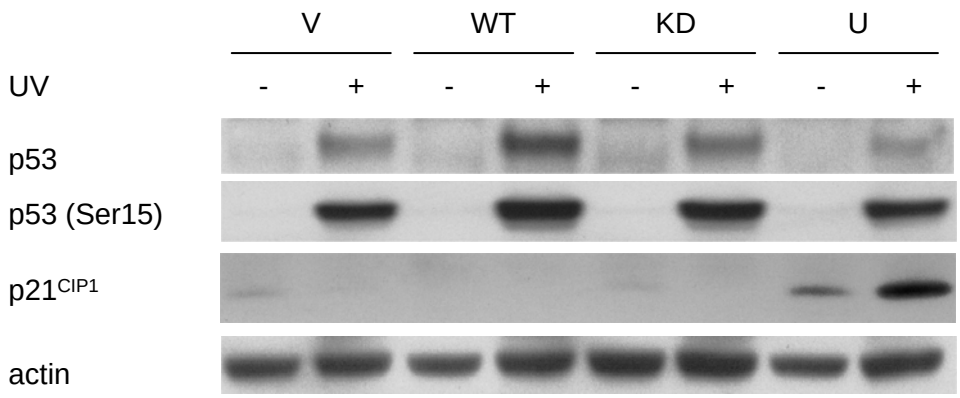

Ji, Ramsey et al., Supplementary Figure 7

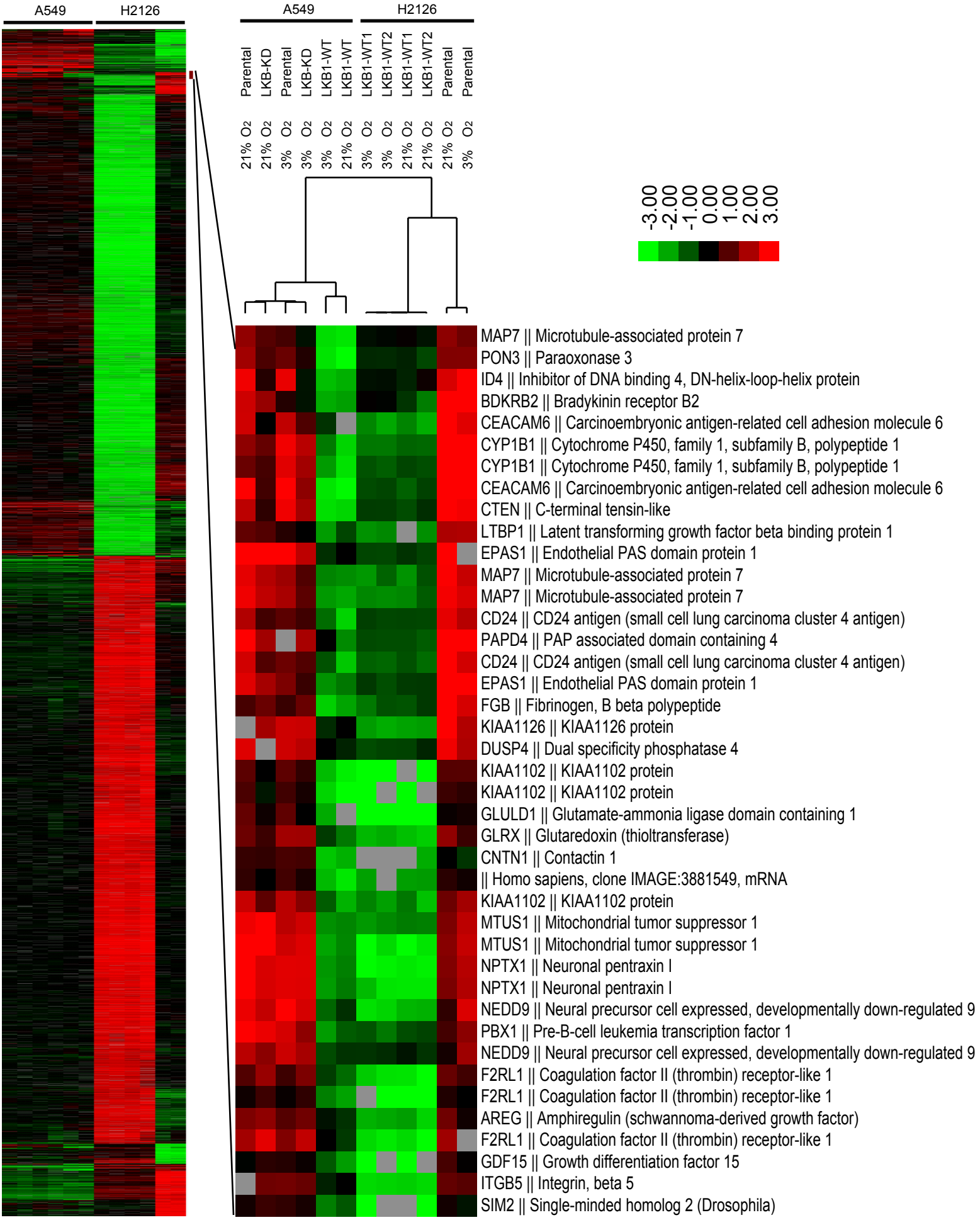

Ji, Ramsey et al., Supplementary Figure 8

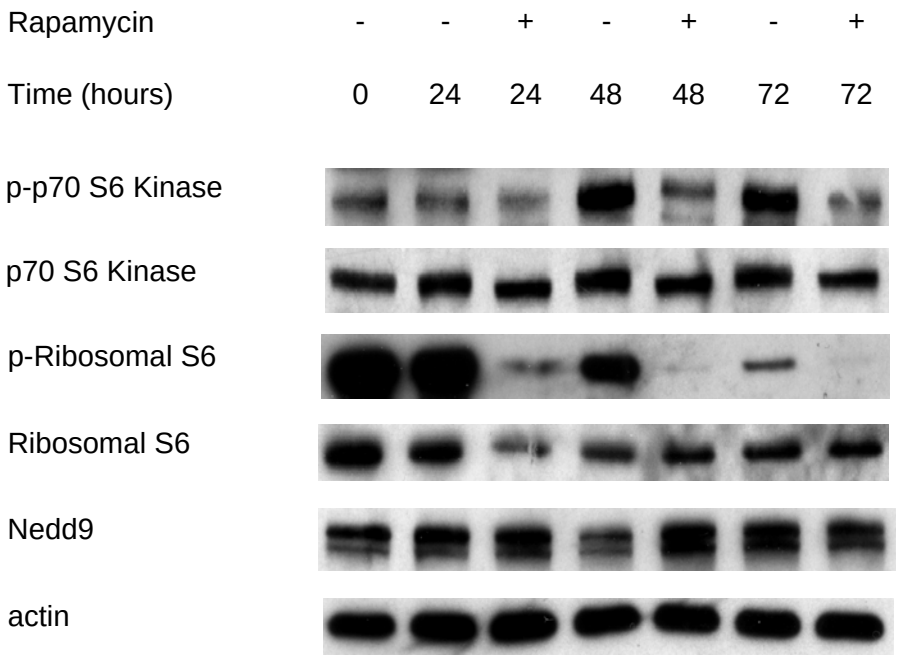

Ji, Ramsey et al., Supplementary Figure 9

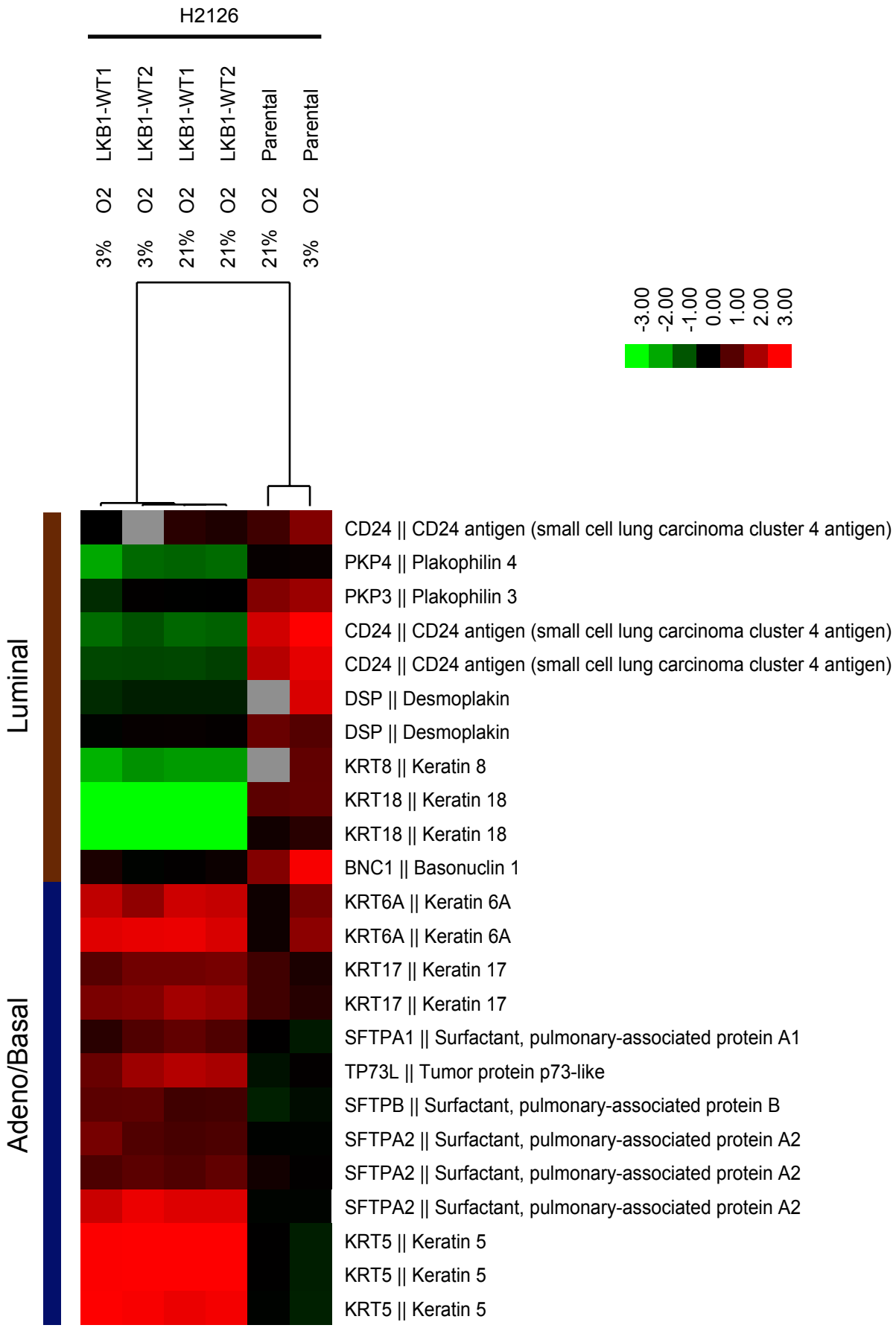

Ji, Ramsey et al., Supplementary Figure 10

A549

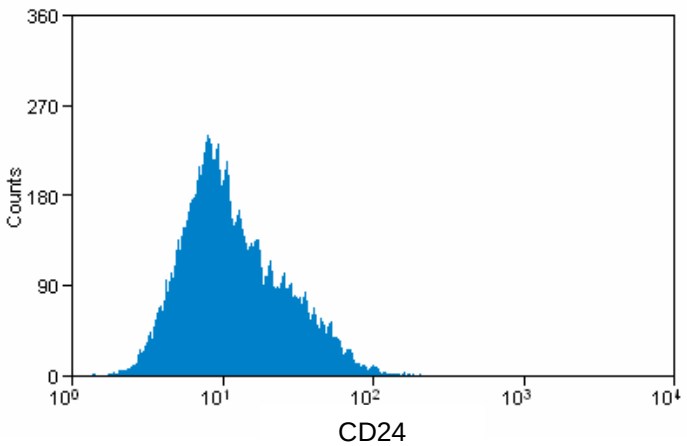

H2126

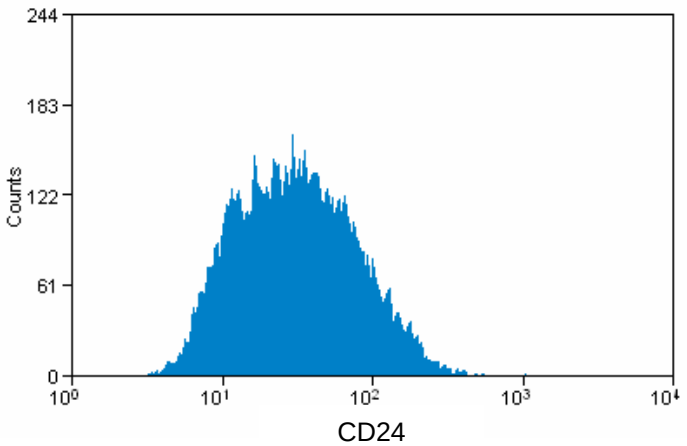

A549
+LKB1-WT

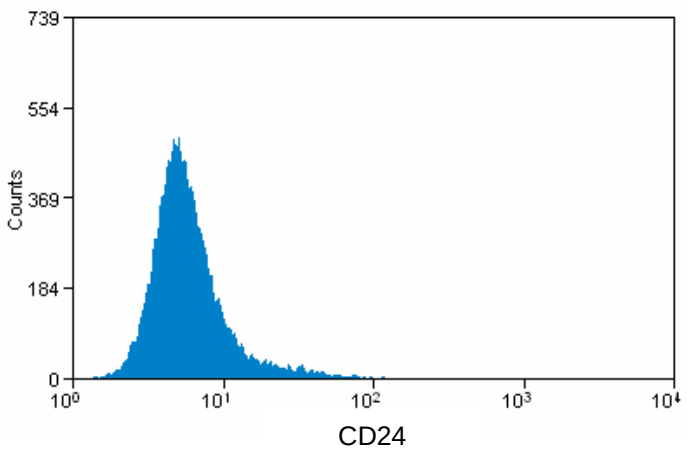

H2126
+LKB1-WT

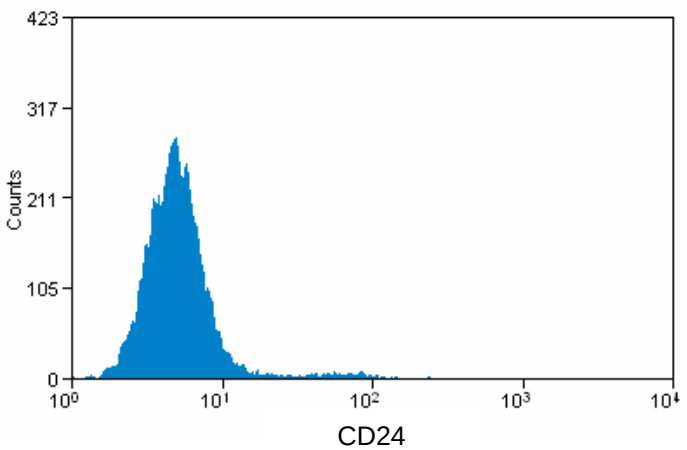

Ji, Ramsey et al., Supplementary Figure 11

SUPPLEMENTARY LEGENDS

Supplementary Figure 1: Heterogeneous activation of conditional β-gal in the lung

Whole mount (top) and eosin stained (bottom) lung from Rosa26-LSL-LacZ mice 1 month after inhalation of indicated adenovirus. β-galactosidase staining (blue) indicates infection, with preference for lower lobes and large airways.

Supplementary Figure 2: Conditional excision of *Lkb1* cooperates with K-ras activation in murine lung tumor initiation and progression

a. Tumor-free survival of mice treated with adeno-CRE. Cohort consists of *K-ras* (n=26), *K-ras Lkb1*$^{+/-\text{ or } L/+}$ (n=27), *K-ras Lkb1*$^{L/-\text{ or } L/L}$ (n=56), and *Lkb1*$^{L/-\text{ or } L/L}$ (n=15). P<0.002 for pair-wise comparison between *K-ras* and *K-ras Lkb1*$^{+/-\text{ or } L/+}$, and p<0.0001 for pair-wise comparison between *K-ras* and *K-ras Lkb1* $^{L/-\text{ or } L/L}$.

b. Representative histology of lesions in *K-ras* or *K-ras Lkb1*$^{L/-}$ mice treated with adeno-CRE at 2 weeks (top) or 4 weeks (bottom) after treatment. Photographs are 100X original magnification.

c. Mice lacking Lkb1 have increased metastasis. Representative photographs of lymph node metastasis from *K-ras Lkb1*$^{L/-}$ mice. Dissection showed that this was a lymph node separate from the lung itself. Note the adenocarcinoma histology, which was found in all metastatic lesions.

Supplementary Figure 3: MLPA analyses of human lung cancers.

Normalized peak height graphs for *LKB1* MLPA. Each bar represents the normalized peak height for the probe indicated on the X axis, with control probes

first, then probes in genomic order from 0.9 Mb 5' to *LKB1* to 10 Mb 3' to *LKB1*, including probes for each exon of *LKB1*. Graphs are shown from representative NSCLC samples with normal copies of *LKB1* (a), single copy loss of the whole *LKB1* allele (b) and single copy loss of the whole *LKB1* allele plus homozygous loss of exons 7 and 8 (c).

Supplementary Figure 4: Lkb1 induces transcription of the *Ink4a/Arf* locus

a. Excision of *Lkb1* reduces accumulation of $p16^{Ink4a}$ and Arf protein in $Lkb1^{L/-}$ MEFs. Western blot analysis of Lkb1, $p16^{Ink4a}$, and Arf protein levels at various times after adenoviral treatment. Actin serves as a loading control. * designates a non-specific background band. Arrow designates Arf protein.

b. Excision of *Lkb1* reduces accumulation of $p16^{Ink4a}$ and *Arf* mRNA in $Lkb1^{L/-}$ MEFs. Taqman Real-Time PCR analysis of $p16^{Ink4a}$ or *Arf* levels in $Lkb1^{L/-}$ MEFs 16 days after conditional excision of *Lkb1* by adenoviral-CRE. Values represent ratio of mRNA levels in $Lkb1^{L/-}$ (treated with adeno-empty) to mRNA levels in $Lkb1^{-/-}$ (treated with Adeno-CRE). Data represent 4 independent experiments. Error bars represent $^{+}$/- SEM.

Supplementary Figure 5: Microarray analysis of murine tumors

Microarray analysis of K-ras-induced lung tumors of the indicated genotypes. Unsupervised hierarchical clustering was performed on 3,275 unique and dynamic transcripts (left). Excerpted gene clusters are shown at the right. Genes in blue

are overexpressed in human SCC and genes in red are known regulators of metastasis. Lkb1 (Stk11) and CD24 are also indicated.

Supplementary Figure 6: Validation of microarray data

Immunohistochemical analysis of Lkb1 pathway activation in lung tumors from *Kras* (left) or *Kras Lkb1*$^{L/-}$ (right) mice. Note that tumors lacking *Lkb1* have reduced phosphorylation of AMPK and ACC, but have increased phosphorylation of S6 kinase. *Kras Lkb1*$^{L/-}$ tumors also show increased Vegf-c staining, consistent with increased transcription seen in microarray analysis.

Supplementary Figure 7: Reconstitution of either WT LKB1 or LKB1 KD has no impact upon the p53 response to UV in A549 cells

A549 cells stably transduced with either pBABE-puro (V), pBABE – LKB1 (WT), or kinase dead pBABE – LKB1^{K78D} (KD) were treated with 40 J/m^2 UV, then assessed after 24 hours for p53, p21^{CIP1}, and phospho-p53 (Ser 15) levels. The UACC-257 melanoma cell line (U) serves as a positive control. Actin serves as a loading control.

Supplementary Figure 8: Microarray analysis of the impact of LKB1 in A549 and H2126 cell lines

A549 and H2126 parental cell lines as well as their derivative lines reconstituted with wild type LKB1 or kinase dead LKB1 (KD) were cultured in 3% and 21% oxygen conditions because of concerns for potential interaction between LKB1 and oxygen sensing pathways. Two-way unsupervised hierarchical clustering was

performed on 9644 unique and dynamic transcripts (left). Excerpted gene clusters are shown at the right. The transcripts from the different cell lines clustered together based on the presence or absence of *LKB1* irrespective of oxygen culture conditions. Notice that NEDD9 expression in top right panel is strongly regulated by the WT LKB1 reconstitution but not by the LKB1 KD.

Supplementary Figure 9: Treatment with rapamycin does not affect expression of NEDD9

Treatment with rapamycin does not affect expression of NEDD9. A549 cells were treated with 100nM rapamycin for indicated time and assessed for expression of indicated genes by western blotting. Actin serves as a loading control.

Supplementary Figure 10: Microarray analysis of H2126 cell lines

H2126 parental cell line and two independently derived lines reconstituted with wild type LKB1 were cultured in 3% and 21% oxygen conditions because of concerns for potential interaction between LKB1 and oxygen sensing pathways. Two-way unsupervised hierarchical clustering was performed on 9644 unique and dynamic transcripts, and an excerpted gene cluster is shown.

Supplementary Figure 11: FACS analysis of CD24 expression

A549 (left) and H2126 (right) parental cell lines (top) and their derivative lines reconstituted with wild type LKB1 (bottom) were assessed for cell surface expression of CD24 by FACS.

Supplementary File 1: All genes used for microarray clustering in mouse lung tumors with indicated genotype

List of 3275 filtered and collapsed transcripts used for hierarchical clustering in Figure 2. File is in .cdt format which can be opened with Microsoft Excel or TreeView.

Supplementary File 2: All genes used for microarray clustering in both A549 and H2126 cells with constitution of with either WT LKB1 or LKB1 KD.

List of 9644 filtered and collapsed transcripts used for hierarchical clustering in Supplementary Figure 7. File is in .cdt format which can be opened with Microsoft Excel or TreeView.

SUPPLEMENTARY TABLES:

Supplementary Table 1. Copy number alterations and mutations in LKB1 in human tumors analyzed by MLPA and direct sequencing

Sample	Histology	LKB1 MLPA	Direct Sequencing	Amino acid change
Ad-1	ADC	Single copy loss	544_546del CTG	Deletion of A.A. 182
Ad-2	ADC	Single copy loss	647T>C	S216F
Ad-3	ADC	Single copy loss	IVS3-1G>A	
Ad-4	ADC	Single copy loss	IVS5-2A>T;	
Ad-5	ADC	Single copy loss and del e7-e8	no mutations	
Ad-6	ADC	del e2-e3	no mutations	
Ad-7	ADC	del p1-e1	no mutations	
Ad-8	ADC	del p1-e1	no mutations	
Ad-9	ADC	Single copy loss	no mutations	
Ad-10	ADC	Single copy loss	no mutations	
Ad-11	ADC	Single copy loss	no mutations	
Ad-12	ADC	Single copy loss	no mutations	
Ad-13	ADC	Single copy loss	no mutations	
Ad-14	ADC	Single copy loss	no mutations	
Ad-15	ADC	Single copy loss	no mutations	
Ad-16	ADC	Single copy loss	no mutations	
Ad-17	ADC	Single copy loss	no mutations	
Ad-18	ADC	Single copy loss	no mutations	
Ad-19	ADC	Single copy loss	no mutations	
Ad-20	ADC	failed	IVS1+2T>G;	
Ad-21	ADC	no mutations	165_166insT	FS, truncates
Ad-22	ADC	no mutations	208G>T	E70X
Ad-23	ADC	no mutations	580G>A	D194N
Ad-24	ADC	no mutations	584_585insT	FS, truncates
Ad-25	ADC	no mutations	724G>C	242G>R
Ad-26	ADC	no mutations	825_827delG	FS, truncates
Ad-27	ADC	no mutations	IVS4-2A>T	
Ad-28	ADC	amplification	no mutations	
Ad-29	ADC	no mutations	no mutations	
Ad-30	ADC	no mutations	no mutations	

Ad-31	ADC	no mutations	no mutations	
Ad-32	ADC	no mutations	no mutations	
Ad-33	ADC	no mutations	no mutations	
Ad-34	ADC	no mutations	no mutations	
Ad-35	ADC	no mutations	no mutations	
Ad-36	ADC	no mutations	no mutations	
Ad-37	ADC	no mutations	no mutations	
Ad-38	ADC	no mutations	no mutations	
Ad-39	ADC	no mutations	no mutations	
Ad-40	ADC	no mutations	no mutations	
Ad-41	ADC	no mutations	no mutations	
Ad-42	ADC	no mutations	no mutations	
Ad-43	ADC	no mutations	no mutations	
Ad-44	ADC	no mutations	no mutations	
Ad-45	ADC	no mutations	no mutations	
Ad-46	ADC	no mutations	no mutations	
Ad-47	ADC	no mutations	no mutations	
Ad-48	ADC	no mutations	no mutations	
Ad-49	ADC	no mutations	no mutations	
Ad-50	ADC	no mutations	no mutations	
Ad-51	ADC	no mutations	no mutations	
Ad-52	ADC	no mutations	no mutations	
Ad-53	ADC	no mutations	no mutations	
Ad-54	ADC	no mutations	no mutations	
Ad-55	ADC	no mutations	no mutations	
Ad-56	ADC	no mutations	no mutations	
Ad-57	ADC	no mutations	no mutations	
Ad-58	ADC	no mutations	no mutations	
Ad-59	ADC	no mutations	no mutations	
Ad-60	ADC	no mutations	no mutations	
Ad-61	ADC	no mutations	no mutations	
Ad-62	ADC	no mutations	no mutations	
Ad-63	ADC	no mutations	no mutations	
Ad-64	ADC	no mutations	no mutations	
Ad-65	ADC	no mutations	no mutations	
Ad-66	ADC	no mutations	no mutations	
Ad-67	ADC	no mutations	no mutations	
Ad-68	ADC	no mutations	no mutations	
Ad-69	ADC	failed	no mutations	

Ad-70	ADC	failed	no mutations	
Ad-71	ADC	failed	no mutations	
Ad-72	ADC	failed	no mutations	
Ad-73	ADC	failed	no mutations	
Ad-74	ADC	failed	no mutations	
Ad-75	ADC	failed	no mutations	
Ad-76	ADC	failed	no mutations	
Ad-77	ADC	failed	no mutations	
Ad-78	ADC	failed	no mutations	
Ad-79	ADC	failed	no mutations	
Ad-80	ADC	failed	no mutations	
SCC-1	SCC	Single copy loss and del e2	no mutations	
SCC-2	SCC	del e8	no mutations	
SCC-3	SCC	Single copy loss	no mutations	
SCC-4	SCC	Single copy loss	no mutations	
SCC-5	SCC	no mutations	Intron 2 del & Exon 3 del 55	FS, truncates
SCC-6	SCC	no mutations	838_843insC	FS, truncates
SCC-7	SCC	no mutations	487G>T	G163C
SCC-8	SCC	failed	368A>G	Q123R
SCC-9	SCC	no mutations	no mutations	
SCC-10	SCC	no mutations	no mutations	
SCC-11	SCC	no mutations	no mutations	
SCC-12	SCC	no mutations	no mutations	
SCC-13	SCC	no mutations	no mutations	
SCC-14	SCC	no mutations	no mutations	
SCC-15	SCC	no mutations	no mutations	
SCC-16	SCC	no mutations	no mutations	
SCC-17	SCC	no mutations	no mutations	
SCC-18	SCC	no mutations	no mutations	
SCC-19	SCC	no mutations	no mutations	
SCC-20	SCC	no mutations	no mutations	
SCC-21	SCC	no mutations	no mutations	
SCC-22	SCC	no mutations	no mutations	
SCC-23	SCC	no mutations	no mutations	
SCC-24	SCC	no mutations	no mutations	
SCC-25	SCC	no mutations	no mutations	
SCC-26	SCC	no mutations	no mutations	
SCC-27	SCC	no mutations	no mutations	

SCC-28	SCC	no mutations	no mutations	
SCC-29	SCC	no mutations	no mutations	
SCC-30	SCC	no mutations	no mutations	
SCC-31	SCC	no mutations	no mutations	
SCC-32	SCC	no mutations	no mutations	
SCC-33	SCC	failed	no mutations	
SCC-34	SCC	failed	no mutations	
SCC-35	SCC	failed	no mutations	
SCC-36	SCC	failed	no mutations	
SCC-37	SCC	failed	no mutations	
SCC-38	SCC	failed	no mutations	
SCC-39	SCC	failed	no mutations	
SCC-40	SCC	failed	no mutations	
SCC-41	SCC	failed	no mutations	
SCC-42	SCC	failed	no mutations	
Other-1	Ad-Sq	Single copy loss	no mutations	
Other-2	Ad-Sq	failed	no mutations	
Other-3	Ad-Sq	failed	no mutations	
Other-4	Ad-Sq	no mutations	no mutations	
Other-5	Ad-Sq	no mutations	no mutations	
Other-6	LCC	duplication	no mutations	
Other-7	LCC	failed	no mutations	
Other-8	LCC	failed	no mutations	
Other-9	LCC	failed	no mutations	
Other-10	LCC	no mutations	no mutations	
Other-11	LCC	no mutations	no mutations	
Other-12	LCC	no mutations	no mutations	
Other-13	LCC	no mutations	no mutations	
Other-14	LCC	no mutations	no mutations	
Other-15	LCC	no mutations	no mutations	
Other-16	LCC	no mutations	no mutations	
Other-17	Unknown	failed	1225C>T	R409W
Other-18	Unknown	failed	no mutations	
Other-19	Unknown	no mutations	no mutations	
Other-20	Unknown	no mutations	no mutations	
Other-21	Unknown	no mutations	no mutations	
Other-22	Unknown	no mutations	no mutations	

Supplementary Table 2. A compilation of K-Ras mutation from nearly seven thousand tumors from the COSMIC database at the Sanger Center [1]

Histology	Mutant	Sequenced	Frequency
Adenosquamous	12	92	13%
Squamous cell	72	1199	6%
Large cell	36	158	23%
Bronchioloalveolar	56	197	28%
Adenocarcinoma	901	3957	23%
NSCLCa-unspecified	301	1300	23%

Supplementary Table 3. Correlation of p53 or K-RAS mutation with LKB1 mutation in primary NSCLC-adenocarcinoma.

		Number (%)	LKB1 MUT (%)	LKB1 WT (%)
K-RAS Mutation	+	21 (26)	8 (10)	13 (16)
	-	59 (74)	19 (24)	40 (50)
p53 Mutation	+	24 (30)	8 (10)	16 (20)
	-	56 (70)	19 (24)	37 (46)

Supplementary Table 4. Correlation of p53 or K-RAS mutation with LKB1 mutation in primary NSCLC-squamous cell carcinomas.

		Number (%)	LKB1 MUT (%)	LKB1 WT (%)
K-RAS Mutation	+	4 (9)	1 (2)	3 (7)
	-	38 (91)	7 (17)	31 (74)
p53 Mutation	+	15 (36)	5 (12)	10 (24)
	-	27 (64)	3 (7)	24 (57)

Supplementary Table 5. Correlation of p53 or K-RAS mutation with LKB1 mutation in primary NSCLC-other sub-types (large cell, adenosquamous, unknown).

		Number (%)	LKB1 MUT (%)	LKB1 WT (%)
K-RAS Mutation	+	1 (5)	0	1 (5)
	-	21 (95)	2 (9)	19 (86)
p53 Mutation	+	7 (32)	0	7 (32)
	-	15 (68)	2 (9)	13 (59)

Supplementary Table 6. Correlation of p53 with K-RAS mutation by NSCLC sub-type.

		K-RAS WT (%)	K-RAS MUT (%)
Adeno	p53 WT	45 (56)	11 (14)
	p53 Mutant	14 (18)	10 (12)
SCC	p53 WT	26 (62)	1 (2)
	p53 Mutant	12 (29)	3 (7)
Other	p53 WT	15 (68)	0
	p53 Mutant	6 (27)	1 (5)

Supplementary Table 7: Tumors used for RNA expression analysis in Supplementary Figure 5.

Mouse #	Label in Fig. 3	Genotype	Histology
405	Tumor A	LSL-Kras	Adenocarcinoma
196-T1	Tumor B	LSL-Kras, $p53^{L/L}$	Adenocarcinoma
186-T1	Tumor C	LSL-Kras, $p53^{L/L}$	Adenocarcinoma
500-T1	Tumor D	LSL-Kras, $p53^{L/L}$	Adenocarcinoma
197-T1	Tumor E	LSL-Kras, $p53^{L/L}$	Adenocarcinoma
91-T1	Tumor F	LSL-Kras, $p16^{Ink4a}$-/-	Adenocarcinoma
14-T1	Tumor G	LSL-Kras, $p16^{Ink4a}$-/-	Adenocarcinoma
498 (1)-T1	Tumor H	LSL-Kras, $p53^{L/L}$	Adenocarcinoma
268-T1	Tumor I	LSL-Kras	Adenocarcinoma
498 (2)-T1	Tumor J	LSL-Kras	Adenocarcinoma
484	Tumor K	LSL-Kras	Adenocarcinoma
287	Tumor L	LSL-Kras	Adenocarcinoma
459-T1	Tumor M	LSL-Kras , $Lkb1^{L/-}$	Adenocarcinoma
547-T1	Tumor N	LSL-Kras , $Lkb1^{L/-}$	Adenocarcinoma
592-T1	Tumor O1	LSL-Kras, $Lkb1^{L/L}$	Adenocarcinoma
392-T1	Tumor P1	LSL-Kras, $Lkb1^{L/+}$	Adenocarcinoma
861-T1	Tumor Q	LSL-Kras, $Lkb1^{L/L}$	Adenocarcinoma
392-T2	Tumor P2	LSL-Kras, $Lkb1^{L/+}$	Adenocarcinoma
592-T2	Tumor O2	LSL-Kras, $Lkb1^{L/L}$	Adenocarcinoma
592-M	Tumor O3	LSL-Kras, $Lkb1^{L/L}$	Adenocarcinoma, metastasis
452-T2	Tumor R1	LSL-Kras, $Lkb1^{L/-}$	Adenosquamous carcinoma
452-T1	Tumor R2	LSL-Kras, $Lkb1^{L/-}$	Adenosquamous carcinoma
113-T1	Tumor S	LSL-Kras, $Lkb1^{L/-}$	Squamous carcinoma
540-T2	Tumor T2	LSL-Kras, $Lkb1^{L/-}$	Squamous carcinoma
540-T1	Tumor T1	LSL-Kras, $Lkb1^{L/-}$	Squamous carcinoma

References

1. Forbes, S. et al. Cosmic 2005. *Br J Cancer* **94**, 318-322 (2006).